

## A hybrid airfoil design method to simulate full-scale ice accretion throughout a given C(l)-range

**Farooq Saeed**

*Illinois Univ., Urbana*

**Michael S. Selig**

*Illinois Univ., Urbana*

**Michael B. Bragg**

*Illinois Univ., Urbana*

**AIAA, Aerospace Sciences Meeting & Exhibit, 35th, Reno, NV, Jan. 6-9, 1997**

A design procedure for hybrid airfoils with full-scale leading edges and redesigned aft-sections that exhibit full-scale airfoil water droplet impingement characteristics throughout a given C(l)-range is presented. The design procedure not only allows for subcritical and viscous flow analysis in the design but also is capable of off-design droplet impingement simulation through the use of a flap system. The limitations of the flap-system based design for simulating both on- and off-design full-scale droplet impingement characteristics and surface velocity distribution are discussed with the help of specific design examples. In particular, the paper presents the design of two hybrid airfoils at two different angles of attack, such that they simulate both full-scale velocity distribution as well as droplet impingement at the respective design angles of attack. Both of the hybrid airfoils are halfscale airfoil models with a 5 percent upper and 20 percent lower full-scale surface of the Learjet 305 airfoil leading edge. The effect of flap deflection and droplet size on droplet impingement characteristics is also presented to highlight the important limitations of the present method both on and off design. The paper also discusses important compromises that must be made in order to achieve full-scale ice accretion simulation throughout a desired C(l)-range. (Author)

## A HYBRID AIRFOIL DESIGN METHOD TO SIMULATE FULL-SCALE ICE ACCRETION THROUGHOUT A GIVEN $C_l$ -RANGE

Farooq Saeed,\* Michael S. Selig† and Michael B. Bragg‡  
 Department of Aeronautical and Astronautical Engineering  
 University of Illinois at Urbana-Champaign  
 Urbana, Illinois 61801

### ABSTRACT

A design procedure for hybrid airfoils with full-scale leading edges and redesigned aft-sections that exhibit full-scale airfoil water droplet impingement characteristics throughout a given  $C_l$ -range is presented. The design procedure is an extension of the method first published by Saeed, et al., in that it not only allows for subcritical and viscous flow analysis in the design but is also capable of off-design droplet impingement simulation through the use of a flap system. The limitations of the flap-system based design for simulating both on- and off-design full-scale droplet impingement characteristics and surface velocity distribution are discussed with the help of specific design examples. In particular, the paper presents the design of two hybrid airfoils at two different angles of attack, such that they simulate both full-scale velocity distribution as well as droplet impingement at the respective design angles of attack. Both of the hybrid airfoils are half-scale airfoil models with a 5% upper and 20% lower full-scale surface of the Learjet 305 airfoil leading-edge. The effect of flap deflection and droplet size on droplet impingement characteristics is also presented to highlight the important limitations of the present method both on and off design. The paper also discusses important compromises that must be made in order to achieve full-scale ice accretion simulation throughout a desired  $C_l$ -range and suggests alternatives such as applying a multipoint design approach for the design.

### NOMENCLATURE

$C_l$  = airfoil lift coefficient  
 $c$  = airfoil chord length  
 $S$  = airfoil surface arc length measured from the leading-edge  
 $T$  = freestream static temperature

$V$  = surface velocity  
 $V_\infty$  = freestream velocity  
 $\bar{V}$  = surface velocity normalized by  $V_\infty$   
 $VMD$  = volume median droplet diameter  
 $x, y$  = airfoil coordinates  
 $\alpha$  = angle of attack relative to the chord line  
 $\alpha_e$  = effective angle of attack relative to the nose-section chord line,  $\alpha - \gamma$   
 $\beta$  = local impingement efficiency  
 $\gamma$  = nose droop angle  
 $\Gamma$  = circulation strength normalized by  $V_\infty c$   
 $\delta$  = droplet diameter  
 $\delta_f$  = flap deflection, deg

#### Subscripts:

$fs$  = full-scale airfoil  
 $l$  = lower surface  
 $ss$  = subscale airfoil  
 $u$  = upper surface

### INTRODUCTION

Recent aircraft accidents have raised important flight safety<sup>1-5</sup> issues related to the operation of aircraft under severe weather conditions. To improve flight safety, a better understanding of the effect of ice accretion on the aerodynamic performance of modern airfoils is required. One important step in the process is to evaluate the aerodynamic performance of the airfoil sections, or the wing as a whole, at the icing conditions within the certification icing envelop that results in the largest performance penalties.

For aircraft safety, one of the most important performance parameters is the maximum lift coefficient. Therefore, while drag and pitching moment are important, the icing condition that results in the largest degradation in maximum lift coefficient is the most critical icing condition. The determination of the critical ice accretion and its aerodynamic effect on a set of modern airfoils, typical of those in use on aircraft, is underway at NASA Lewis Research Center. The research reported here is part of this larger effort.

Owing to the difficulties and uncertainties in ice accretion scaling,<sup>6-14</sup> testing at full-scale is desirable, yet costly. Moreover, available ice accretion tunnels are too small to test full-scale airfoils or wings of most aircraft of interest. One way to ex-

---

Copyright © 1997 by Farooq Saeed, Michael S. Selig and Michael B. Bragg. Published by the American Institute of Aeronautics and Astronautics, Inc. with permission.

\* Graduate Research Assistant. Student Member AIAA.

† Assistant Professor. Member AIAA.

‡ Professor. Associate Fellow AIAA.

pand the usefulness of existing icing tunnels and to facilitate testing of aircraft deicing/anti-icing systems is to test "hybrid airfoils" or "sub-scale airfoils" with full-scale leading edges and redesigned aft sections to provide full-scale icing conditions at the leading edge. The term "hybrid method" refers to using a full-scale leading edge to match the full-scale ice accretion. The aft section of the hybrid airfoil is specially designed to provide flowfield and droplet impingement similar to that on the full-scale airfoil leading-edge. One such approach<sup>15</sup> used airfoils with full-scale leading edges and truncated aft-sections to simulate the flowfield of the full scale, thereby avoiding the ice-accretion process on the airfoil leading edge and the associated scaling issues altogether. Interestingly, neither the approach, nor its range of application, received much attention despite its numerous merits since it permits an indepth study of droplet impingement and ice accretion on full-scale leading-edge sections within the capabilities of current icing research facilities.

In the absence of a systematic study to provide insight into the design of the aft section, a recent study<sup>16</sup> was carried out in which a design procedure for hybrid airfoils was successfully developed and demonstrated with specific design examples. The study showed that hybrid airfoils could be designed to exhibit both the full-scale velocity distribution on its nose section as well as full-scale droplet-impingement characteristics and, therefore, ice accretion. An inherent limitation of the design procedure outlined in the study<sup>16</sup> is that the method was restricted to a single-point design and, therefore, lacked the capability to handle off-design cases. Moreover, the method used the "matched lift coefficient" technique to correct for viscous effects.

To overcome these limitations, the present study was carried out with the objective to expand the scope of the single-point design procedure of Ref. 16 to a method that enables the hybrid airfoils to exhibit both full-scale velocity distribution as well as droplet impingement and, therefore, ice accretion throughout a desired  $C_l$ -range or a range of angles of attack  $\alpha$ .

The task of simulating off-design full-scale droplet impingement, as will be shown later, is successfully accomplished by introducing a plain flap on the hybrid airfoil. The use of a plain flap, however, fails to simulate full-scale velocity distribution at the off-design conditions. Since the difference in the velocity distribution on the nose section will effect the thermodynamics of ice accretion as the droplets impinge on the surface, it therefore becomes necessary to simulate the full-scale velocity distribution in ad-

dition to droplet impingement at the off-design conditions. Thus, to simulate both the full-scale velocity distribution as well as droplet impingement on the nose section of the hybrid airfoil throughout a desired  $C_l$ -range, it is necessary to formulate a multipoint hybrid airfoil design method.

To set the stage for the multipoint design method, the paper presents the design of two half-scale hybrid airfoils that are designed at two different angles of attack such that they simulate both the full-scale velocity distribution as well as droplet impingement characteristics on the nose sections at their respective design angles of attack. The velocity distribution and droplet impingement characteristics of the two hybrid airfoils are then analyzed at an off-design angle of attack and compared with that of the full-scale airfoil. The results are then used to highlight the limitations of the present method and, therefore, suggest a need for a multipoint design method. Important compromises that must be made to achieve a multipoint design for full-scale ice accretion simulation throughout a desired  $C_l$ -range are also discussed.

## DESIGN APPROACH

The hybrid airfoil design procedure for full-scale flowfield and droplet impingement simulation uses validated computational airfoil aerodynamics and droplet impingement codes,<sup>17-32</sup> specifically, an inverse design method,<sup>32</sup> the Eppler code,<sup>25-27</sup> XFOIL<sup>31</sup> and AIRDROP.<sup>20-22</sup> Reference 16 gives a brief discussion on each of these codes. For a more detailed discussion, the reader is referred to the associated literature.

Unlike the method presented in Ref. 16 where in the potential flow is corrected for viscous effects using the "matched lift coefficient" technique, the present method uses a modified version of XFOIL. The modified version of XFOIL was obtained by integrating the droplet-trajectory and impingement-characteristics calculation subroutines from the AIRDROP code into the XFOIL code. This was especially done to take advantage of XFOIL's ability to analyze both inviscid/viscous flow as well as incompressible/subcritical flows unlike the AIRDROP code, which is purely based on incompressible flow formulation. In this paper, the modified version of XFOIL will be referred to as the XFOIL/AIRDROP code. Once the flowfield is determined using known flight and icing conditions, the droplet trajectory calculation subroutines are then used in conjunction with the flow solver subroutines to determine the water droplet impingement on the airfoil surface.

A conceptual illustration of the hybrid airfoil design procedure is shown in Fig. 1. A brief summary of these steps is as follows. First, a full-scale airfoil geometry is selected and the desired flight and icing conditions are specified. In particular, the Learjet 305 airfoil (shown in Fig. 2) is used in this study to demonstrate the design procedure. The XFOIL/AIRDROP code is then used to predict the limits of droplet impingement. Once the limits of impingement are known on the leading edge of the full-scale airfoil, that part of the full-scale airfoil geometry is fixed for the subsequent hybrid airfoil shapes. As in Ref. 16, this fixed leading-edge section will be referred to as the nose section and the remaining section of the subscale airfoil profile will be referred to as the aft section. The aft section of the hybrid airfoil is then designed to provide full-scale flowfield and droplet impingement characteristics on the nose section of the hybrid airfoil.

An initial geometry for the aft section is obtained through the use of a multipoint inverse airfoil design code<sup>32</sup> (PROFOIL). The design of the intermediate airfoil, from which the aft section of the subscale airfoil is derived, is governed by several constraints, namely, the scale of the subscale airfoil, the upper and lower surface thickness and slope at the junction between the nose and aft sections, and a desired form for the pressure recovery characteristics. Apart from these constraints, additional continuity and closure constraints that form an integral part of the inverse design methodology<sup>32</sup> are also satisfied to achieve a physically realizable design. A multi-dimensional Newton iteration scheme is further employed to satisfy these constraints.

The flow over the hybrid airfoils is then analyzed using the XFOIL/AIRDROP code. In order to have a physically similar flow in the vicinity of the nose section of both the hybrid and the full-scale airfoils, the analysis is performed at the same angle of attack relative to the nose-section chord of both the airfoils. The local velocity distributions over the nose section and the stagnation point locations on both the hybrid and full-scale airfoils are then compared. If the desired velocity distribution over the nose section and stagnation point location are not achieved, the aft section of the hybrid airfoil is redesigned and again merged with the nose section to form a new hybrid airfoil. The flow over the new hybrid airfoil is then analyzed and compared with that over the full-scale airfoil. The process is repeated until the desired velocity distribution over the nose section is achieved.

In the next step, the water droplet trajectories and water droplet impingement characteristics are

determined from the XFOIL/AIRDROP code. The individual droplet trajectories are combined to calculate the droplet impingement characteristics of the airfoil. The droplet impingement characteristics of both the full-scale and the hybrid airfoil are then compared. If the agreement in the droplet impingement characteristics is poor, the hybrid airfoil is modified and the design process is repeated again until good agreement is reached. At this stage, the single-point design is accomplished. To achieve off-design full-scale ice accretions or droplet impingement characteristics, a plain flap is employed on the hybrid airfoil. Thus, by deflecting the flap, the desired droplet impingement characteristics are achieved over the hybrid airfoil for the off-design cases.

The off-design cases reveal, as will be shown in the next section, certain important limitations of the design method. These limitations include 1) the onset of flow separation on the hybrid airfoils at moderate to high angles of attack conditions and 2) a mismatch in the velocity distribution on the nose section at off-design angles of attack. The former limitation can be improved either by using a more sophisticated flap system or by applying less conventional techniques such as boundary-layer control through slot suction<sup>33,34</sup> or circulation control via trailing-edge blowing. The latter, however, is an important limitation of the present design method and can be overcome by using a multipoint design approach.

## IMPLEMENTATION

In this section, the effects of various parameters on two single-point airfoil designs are discussed. In particular, two half-scale hybrid airfoils were designed at different angles of attack such that they simulated both the full-scale velocity distribution on the nose section as well as droplet impingement characteristics at the design conditions (single-point design). The off-design full-scale velocity distribution and droplet impingement simulation characteristics of each hybrid airfoil are compared to highlight important limitations of the present method.

### Single-Point Design and Simulation

The design of two half-scale models of the GLC 305 airfoil that simulate full-scale velocity distribution and droplet impingement is presented. Of the two hybrid airfoils A and B, hybrid airfoil A is designed to simulate full-scale ice accretion at  $\alpha = 2$  deg while hybrid airfoil B is designed to simulate full-scale ice accretion at  $\alpha = 6$  deg along with the icing conditions:  $V_\infty = 90$  m/s (175 kt),  $T = -10^\circ\text{C}$ ,  $Re = 6 \times 10^6$ ,  $M = 0.28$  and  $VMD = 20\mu\text{m}$ . While it is realized that in flight the conditions will change

Table 1 Design flight and icing conditions.

Variable	Full scale	Hybrid A	Hybrid B
$V_\infty$ , m/s	90	90	90
$T$ , deg C	-10	-10	-10
$Re$	$6 \times 10^6$	$3 \times 10^6$	$3 \times 10^6$
$M$	0.28	0.28	0.28
$c$ , m	1.0	0.5	0.5
$VMD$ , $\mu\text{m}$	20	20	20
$\alpha$ , deg	2, 6	2	6
$\gamma$ , deg	0	-1.5	-3
$\alpha_e$ , deg	2, 6	3.5	9

with angle of attack, the conditions for both angles are held constant here to simply illustrate the method.

As a first step, the droplet impingement efficiency  $\beta$  for the GLC 305 airfoil corresponding to the given flight and icing conditions is determined by the XFOIL/AIRDROP code. The results are shown in Fig. 3. For  $\alpha = 6$  deg, the XFOIL/AIRDROP code predicts the maximum limits of impingement as  $S_u = 0.0076$  ( $x/c = 0.0019$ ) on the upper surface and  $S_l = -0.1822$  ( $x/c = 0.1738$ ) on the lower surface. Since the limits of impingement define the surface over which ice will accrete on the airfoil, only that part of the full-scale airfoil geometry needs be fixed as the nose section for the hybrid airfoil. Thus, the nose-section geometry for both the hybrid airfoils was selected as the full-scale airfoil surface from  $x/c = 0.05$  on the upper surface to  $x/c = 0.20$  on the lower surface. The two hybrid airfoils were then designed following the procedure illustrated in Fig. 1. Table 1 lists the flight and icing conditions for the final single-point design.

A comparison of the full-scale airfoil velocity distribution with that of the individual hybrid airfoil velocity distributions (Figs. 4a and 5a) at the single-point design conditions shows good agreement over the common nose section. Comparisons of the impingement characteristics (Figs. 4b and 5b) and tangent droplet trajectories (Figs. 4c and 5c) also indicate excellent agreement with that of the full-scale. The tangent droplet trajectories, although originating from different locations upstream are matched in the vicinity of the leading edge. This is consistent with the observations made during the case studies in Ref. 16. At this point, the single-point design for full-scale velocity distribution and droplet impingement simulation is complete and the two hybrid airfoils along with the Learjet 305 airfoil are shown in Fig. 6.

#### Effect of Droplet Size

The impingement characteristics, i.e., the lim-

its of impingement, the impingement efficiency  $\beta$  ( $\beta$ -curve) and the maximum point on the  $\beta$ -curve, referred to as  $\beta_{max}$ , of an airfoil depend to a large extent on the size of the water droplets in the flow. In the case of small droplets, the droplet drag dominates and the particle is very responsive to the flowfield acting almost as a flow tracer; whereas, in the case of large droplets, the droplet inertia dominates and the particle is less sensitive to changes in the flowfield. Thus, an increase in the droplet size results in an increase in the impingement efficiency  $\beta$ ,  $\beta_{max}$  and the limits of impingement. It, therefore, becomes necessary to examine the effect of different droplet size on full-scale droplet impingement simulation. Since, in an actual icing cloud, the water droplets have diameters ranging from 5-50  $\mu\text{m}$ , the impingement characteristics of the hybrid airfoil A were determined for two different droplet sizes. The results are presented in Fig. 7 and show good agreement where the droplet sizes are less than that selected for the single point design. For larger droplet size, a good overall agreement can be seen, however, the limits of impingement and  $\beta_{max}$  differ slightly.

#### Off-Design Simulation

To simulate full-scale ice accretion or droplet impingement characteristics throughout a desired  $C_l$ - or  $\alpha$ -range, a flap system was employed on each of the hybrid airfoils. The objective was to match both the velocity distribution as well as the droplet impingement characteristics at any off-design angle of attack by an appropriate amount of flap deflection. To accomplish this task, the two hybrid airfoils were analyzed at off-design angles of attack, in particular, the hybrid airfoil A designed to simulate conditions at  $\alpha = 2$  deg was analyzed at  $\alpha = 6$  deg while the hybrid airfoil B designed to simulate conditions at  $\alpha = 6$  deg was analyzed at  $\alpha = 2$  deg. The results are shown in Figs. 8 and 9 in which the hybrid airfoil velocity distribution and impingement characteristics are shown with and without the appropriate flap deflection necessary to simulate full-scale droplet impingement. The results show that, although the use of a flap on hybrid airfoils can be very effective in simulating full-scale droplet impingement characteristics at an off-design condition, it is, however, not able to accurately simulate full-scale velocity distribution over the nose section of that hybrid airfoil.

To determine the optimum flap setting, the root-mean-squares difference in local impingement efficiency  $RMS_\beta$  and in normalized surface velocity  $RMS_{\bar{v}}$  were calculated for different angle of attack and flap settings. Mathematically,  $RMS_\beta$  and  $RMS_{\bar{v}}$  are defined as

$$RMS_{\beta} = \|\beta_{fs}(S) - \beta_{ss}(S)\| \quad (1)$$

$$RMS_{\overline{V}} = \|\overline{V}_{fs}(S) - \overline{V}_{ss}(S)\| \quad (2)$$

where  $S_l \leq S \leq S_u$ .

Figures 10a,b show the variation in  $RMS_{\beta}$  and  $RMS_{\overline{V}}$ , respectively, for different angles of attack and flap settings  $\delta_f$  for the hybrid airfoil A designed for  $\alpha = 2$  deg while Figs. 11a,b show similar plots for the hybrid airfoil B designed for  $\alpha = 6$  deg. The optimum flap deflection was then selected as the one that corresponds to the minimum value of  $RMS_{\beta}$ .

The optimum flap settings corresponding to each angle-of-attack case are plotted in Fig. 12a for clarity. Figure 12b, on the other hand, shows a comparison of the circulation  $\Gamma$  of both the hybrid airfoils with that of the full-scale. The results indicate that the hybrid airfoils require less circulation than the full-scale airfoil to simulate full-scale droplet impingement and that the difference between the full-scale and hybrid airfoil circulation is nearly constant until significant flow separation occurs on the hybrid airfoils. Beyond this point, the hybrid airfoil circulation starts to fall off gradually and, therefore, suggests the limit to which a hybrid airfoil can be used to simulate full-scale droplet impingement characteristics.

It is important to note in Figs. 10 and 11 that the  $RMS_{\overline{V}}$  values are an order of magnitude higher than the corresponding  $RMS_{\beta}$ . Although contributions to the  $RMS$  values due to numerical noise cannot be ruled out completely, differences in surface velocity will certainly effect the thermodynamics of ice accretion. Thus, it becomes necessary to incorporate the ice accretion process in the design method in addition to flow and droplet impingement analysis.

The effect of larger droplet size on off-design simulation is shown in Fig. 13. Similar trends can be observed as in the on-design case. Since large sized droplets result in an increase in the limits of impingement, they together with the angle of attack of interest may dictate the size of the nose section and, thus, limit the range of application of the present method.

## CONCLUSIONS

Several important conclusions can be drawn from this study. First, it is shown that it is possible to design hybrid airfoils with full-scale leading edges and redesigned aft-sections that exhibit full-scale airfoil water droplet impingement characteristics throughout a given  $C_l$ -range. The results indicate the usefulness of a flap system in simulating off-design full-scale droplet impingement characteristics. The use

of flap for full-scale droplet impingement simulation is, however, restricted to low and moderate angles of attack since at high absolute angles of attack together with high flap deflections, the hybrid airfoils become susceptible to flow separation. This limitation can, however, be overcome by the use of a more sophisticated flap system or by the application of boundary-layer control methods.

The results of off-design simulation also reveal the existence of small differences in surface velocity distribution within the limits of droplet impingement. Since this difference in surface velocity will affect the thermodynamics of ice accretion and prevent full-scale ice accretion simulation, the present method should be modified to include the effects of ice accretion as well into the design of hybrid airfoils.

## ACKNOWLEDGMENTS

This work has been sponsored by NASA Lewis Research Center under grant NCC3-408. We would like to thank Reuben Chandrasekharan of Learjet, Inc. for providing NASA Lewis with the Learjet GLC 305 airfoil used in this study. Also, helpful discussions with Gene Addy, Tom Ratvasky and Tom Bond of NASA Lewis are gratefully acknowledged.

## REFERENCES

- <sup>1</sup>Anon., "Selected Bibliography of NACA-NASA Aircraft Icing Publications," NASA TM 81651, Aug. 1981.
- <sup>2</sup>Anon., "Icing Technology Bibliography," SAE AIR-4015, Warrendale, PA, Nov. 1987.
- <sup>3</sup>Anon., "Aircraft Icing," NASA CP-2086 (FAA-RD-78-109), 1979.
- <sup>4</sup>Brun, R. J., "Icing Problems and Recommended Solutions," AGARDograph 16, Nov. 1957.
- <sup>5</sup>Perkins, P., and Rieke, W., "Aircraft Icing Problems — After 50 Years," AIAA Paper 93-0392, Jan. 1993.
- <sup>6</sup>Hauger, H. H. and Englar, K. G., "Analysis of Model Testing in an Icing Wind Tunnel," Douglas Aircraft Co., Inc., Rep. No. SM 14993, May 1954.
- <sup>7</sup>Sibley, P. J. and Smith, R. E., Jr. "Model Testing in an Icing Wind Tunnel," Lockheed Aircraft Corp., Inc., Rep. No. LR 10981, Oct. 14, 1955.
- <sup>8</sup>Dodson, E. D., "Scale Model Analogy for Icing Tunnel Testing," Boeing Airplane Company, Transport Division, Document No. D66-7976, Mar. 1962.
- <sup>9</sup>Bragg, M. B., Gregorek, G. M., and Shaw, R. J., "An Analytical Approach to Airfoil Icing," AIAA Paper 81-0403, Jan. 1981.
- <sup>10</sup>Bragg, M. B., "Effect of Geometry on Airfoil Icing Characteristics," *Journal of Aircraft*, Vol. 21, No. 7, 1984, pp. 505-511.
- <sup>11</sup>Ruff, G. A., "Verification and Application of

the Icing Scaling Equations," AIAA Paper 86-0481, Jan. 1986.

<sup>12</sup>Bilanin, A. J., "Proposed Modifications to Ice Accretion/Icing Scaling Theory," AIAA Paper 88-0203, Jan. 1988.

<sup>13</sup>Anderson, D. N., "Rime-, Mixed- and Glaze-Ice Evaluations of Three Scaling Laws," AIAA Paper 94-0718, Jan. 1994.

<sup>14</sup>Anderson, D. N., "Methods for Scaling Icing Test Conditions," AIAA Paper 95-0540, Jan. 1995. Also published as NASA TM 106827.

<sup>15</sup>Glahn, U. H. von, "Use of Truncated Flapped Airfoils for Impingement and Icing Tests of Full-Scale Leading-Edge Sections," NACA RM E56E11, Jul. 1956.

<sup>16</sup>Saeed, F., Selig, M. S., and Bragg, M. B., "A Design Procedure for Subscale Airfoils with Full Scale Leading-Edges for Ice Accretion Testing," AIAA Paper 96-0635, Jan. 1996.

<sup>17</sup>Taylor, G. I., "Notes on Possible Equipment and Technique for Experiments on Icing on Aircraft," Aeronautical Research Council, R&M 2024, Jan. 1940.

<sup>18</sup>Glauert, M., "A Method of Constructing the Paths of Raindrops of Different Diameters Moving in the Neighbourhood of (1) a Circular Cylinder, (2) an Aerofoil Placed in a Uniform Stream of Air; and a Determination of the Rate of Deposit of the Drops on the Surface and the Percentage of Drops Caught," Aeronautical Research Council, R&M 2025, Nov. 1940.

<sup>19</sup>Langmuir, I. and Blodgett, K. B., "A Mathematical Investigation of Water Droplet Trajectories," Army Air Forces TR 5418, Feb. 1946 (Contract No. W-33-038-ac-9151 with General Electric Co.). Also available from the Department of Commerce Publication Board as PB No. 27565.

<sup>20</sup>Bragg, M. B., "A Similarity Analysis of the Droplet Trajectory Equation," *AIAA Journal*, Vol. 20, No. 12, 1982, pp. 1681-1686.

<sup>21</sup>Bragg, M. B., "AIRDROP: Airfoil Droplet Impingement Code," to be published, NASA CR.

<sup>22</sup>Bragg, M. B., and Gregorek, G. M., "An Incompressible Droplet Impingement Analysis of Thirty Low and Medium Speed Airfoils," The Ohio State University, Aeronautical and Astronautical Research Laboratory, TR AARL 82-02, Columbus, Ohio, Feb. 1982.

<sup>23</sup>Gent, R. W., "Calculation of Water Droplet Trajectories About an Aerofoil in Steady, Two-Dimensional, Compressible Flow," Royal Aircraft Establishment (RAE) TR 84060, June 1984.

<sup>24</sup>Theodoreson, T., and Garrick, I. E., "General Potential Theory of Arbitrary Wing Sections,"

NACA Report 452.

<sup>25</sup>Eppler, R., "Direct Calculation of Airfoils from Pressure Distribution," NASA TT F-15, 417, Mar. 1974. (Translated from *Ingenieur-Archiv*, Vol. 25, No. 1, 1957, pp. 32-57.)

<sup>26</sup>Eppler, R., and Somers, Dan M., "A Computer Program for the Design and Analysis of Low-Speed Airfoils," NASA TM-80210, Aug. 1980.

<sup>27</sup>Eppler, R., *Airfoil Design and Data*, Springer-Verlag, New York, 1990.

<sup>28</sup>Woan, C. J., "Fortran Programs for Calculating the Incompressible Potential Flow About a Single Element Airfoil Using Conformal Mapping," The Ohio State University, Aeronautical and Astronautical Research Laboratory, TR AARL 80-02, Columbus, Ohio, Jan. 1980.

<sup>29</sup>Drela, M., and Giles, M. B., "ISES: A Two-Dimensional Viscous Aerodynamic Design and Analysis Code," AIAA 87-0424, Jan. 1987.

<sup>30</sup>Drela, M., "Low-Reynolds Number Airfoil Design for the MIT Daedalus Prototype: A Case Study," *Journal of Aircraft*, Vol. 25, No. 8, Aug. 1988.

<sup>31</sup>Drela, M., "XFOIL: An Analysis and Design System for Low Reynolds Number Airfoils," *Lecture Notes in Engineering: Low Reynolds Number Aerodynamics*, T. J. Mueller (ed.), Vol. 54, Springer-Verlag, New York, June 1989, pp. 1-12.

<sup>32</sup>Selig, M. S., and Maughmer, M. D., "A Multipoint Inverse Airfoil Design Method Based on Conformal Mapping," *AIAA Journal*, Vol. 30, No. 5, 1992, pp. 1162-1170.

<sup>33</sup>Saeed, F., and Selig, M. S., "A Multipoint Inverse Design of Airfoils with Slot-Suction," *Journal of Aircraft*, Vol. 33, No. 5, 1996, pp. 708-715.

<sup>34</sup>Saeed, F., and Selig, M. S., "A New Class of Airfoils Using Slot-Suction," AIAA Paper 96-0058, Jan. 1996.

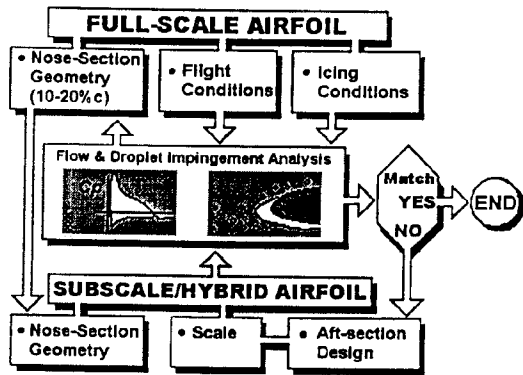


Fig. 1 The subscale/hybrid airfoil design procedure.

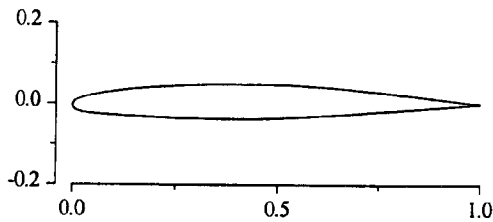


Fig. 2 Learjet 305 (GLC 305) airfoil.

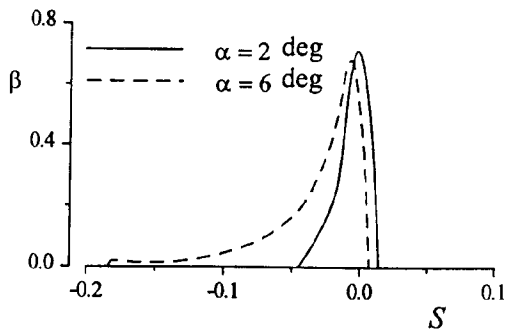


Fig. 3 Droplet impingement efficiency for the Learjet 305 airfoil.

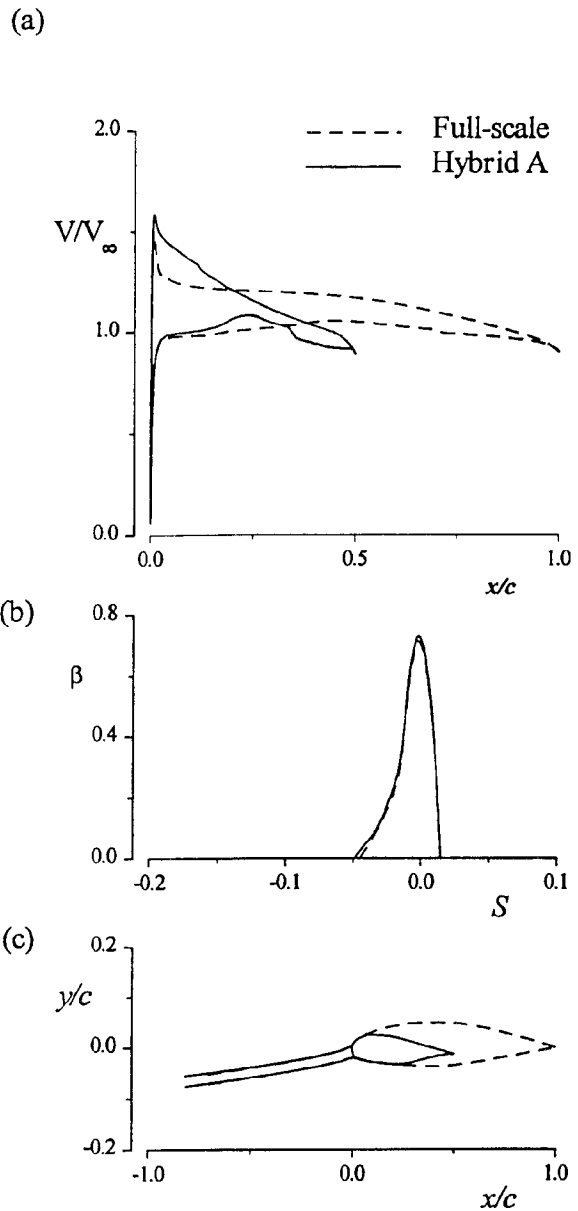


Fig. 4 Comparison of full-scale and hybrid airfoil A (a) velocity distributions, (b) droplet impingement efficiencies and (c) tangent droplet trajectories at the design angle of attack  $\alpha = 2$  deg.



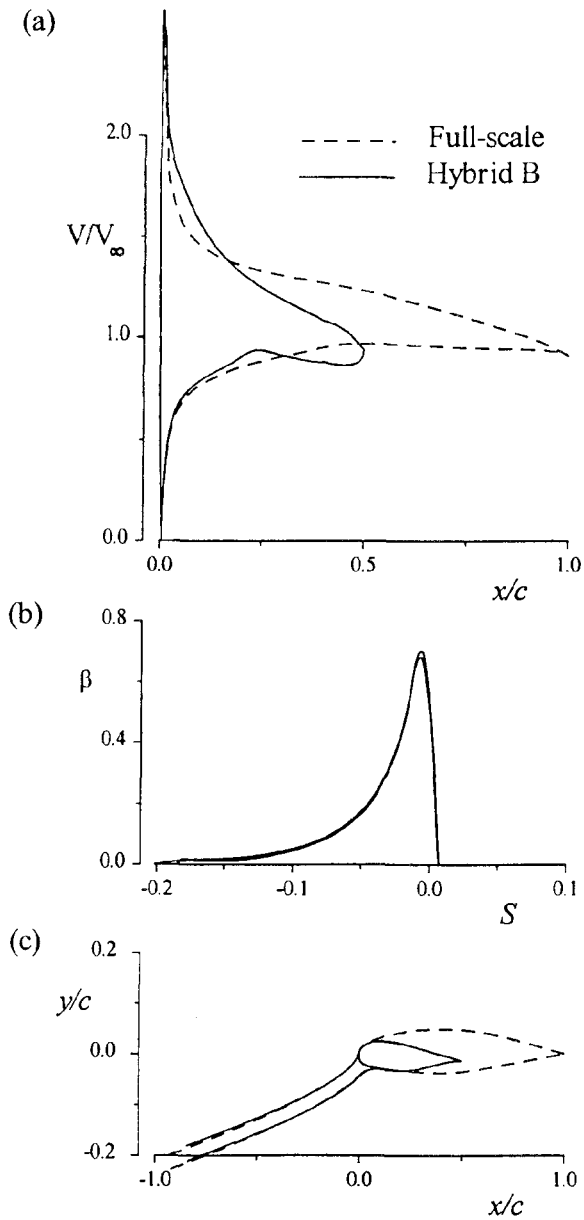


Fig. 5 Comparison of full-scale and hybrid airfoil B (a) velocity distributions, (b) droplet impingement efficiencies and (c) tangent droplet trajectories at the design angle of attack  $\alpha = 6$  deg.

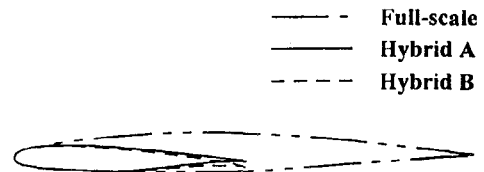


Fig. 6 The two hybrid airfoils and the Learjet 305 airfoil.

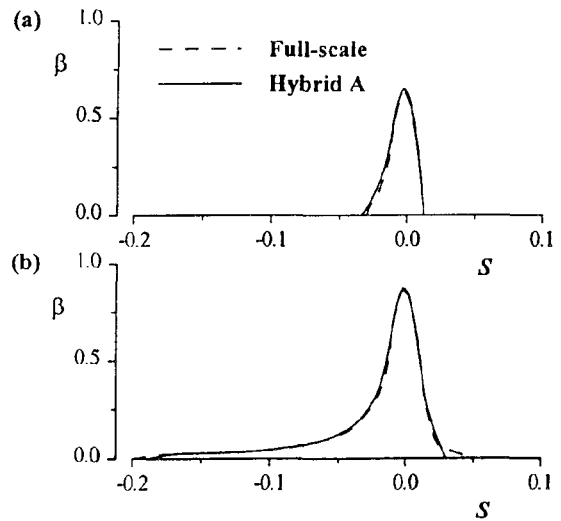


Fig. 7 Comparison of full-scale and hybrid airfoil A droplet impingement efficiencies for (a) 5 micron and (b) 40 micron droplet size at the design angle of attack.

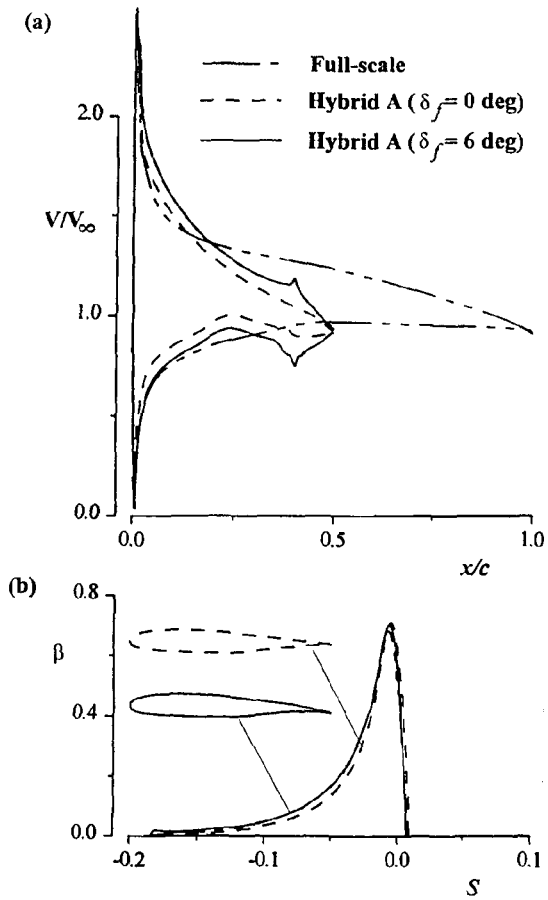


Fig. 8 Comparison of full-scale and hybrid airfoil A (a) velocity distributions and (b) droplet impingement efficiencies at off-design angle of attack  $\alpha = 6$  deg with and without flap deflection.

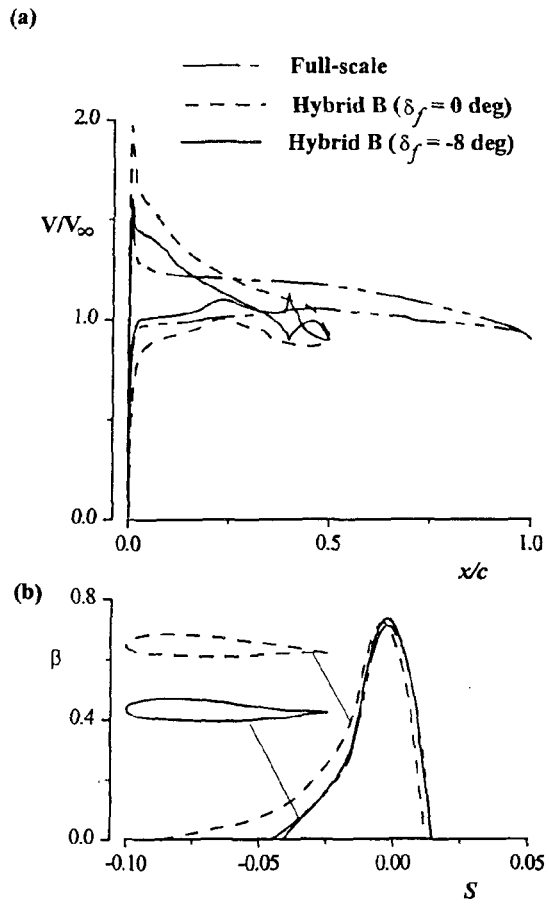


Fig. 9 Comparison of full-scale and hybrid airfoil B (a) velocity distributions and (b) droplet impingement efficiencies at off-design angle of attack  $\alpha = 2$  deg with and without flap deflection.

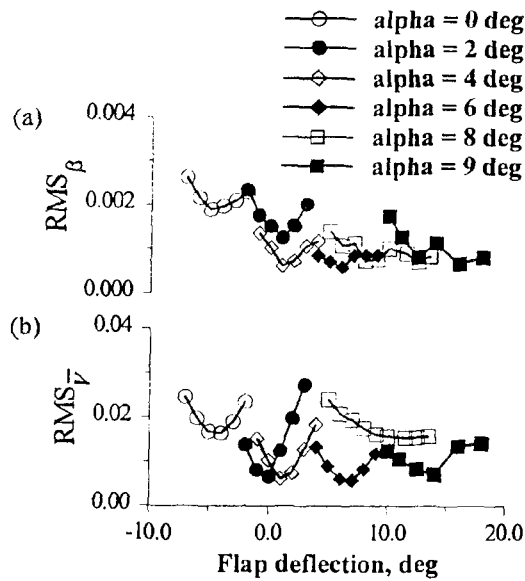


Fig. 10 The variation in the RMS values for different angles of attack and flap settings for the hybrid airfoil A.

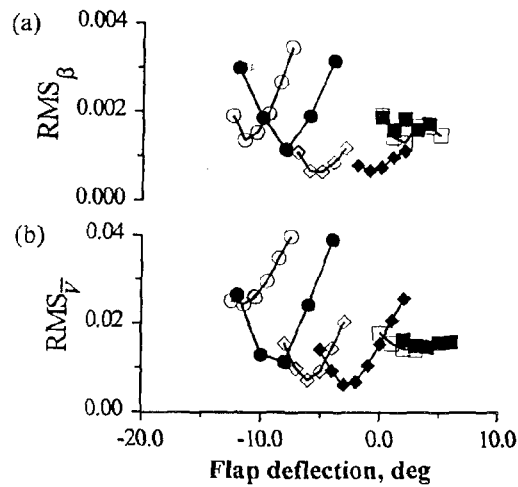


Fig. 11 The variation in the RMS values for different angles of attack and flap settings for the hybrid airfoil B.

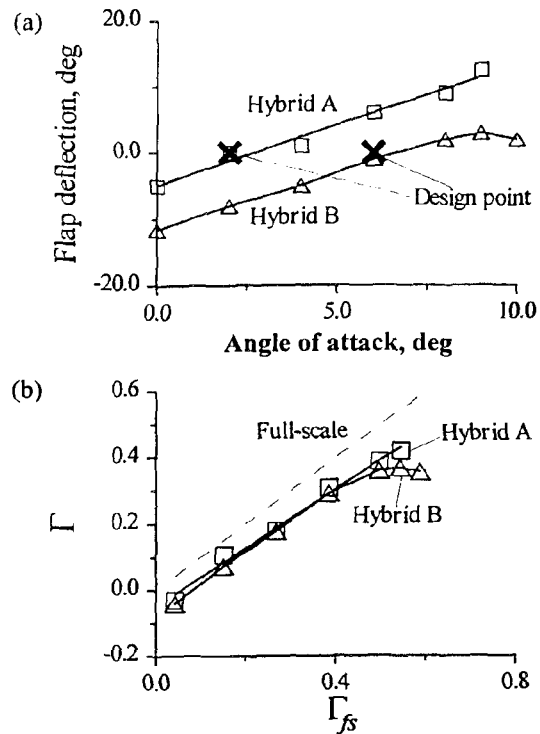


Fig. 12 Plot of (a) the optimum flap deflection and (b) the respective airfoil circulation.

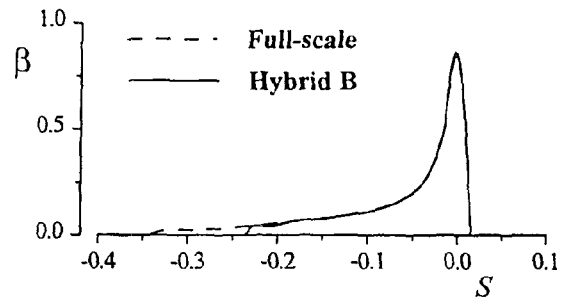


Fig. 13 Comparison of off-design droplet impingement efficiency for 40 micron droplet size at  $\alpha = 4$  deg.